Ionospheric–Thermospheric Responses in South America to the August 2018 Geomagnetic Storm Based on Multiple Observations

Munawar Shah, Ayesha Abbas, Muhsan Ehsan, Andres Calabia Aiber, Binod Adhikari, M. Arslan Tariq, Junaid Ahmed, José Francisco de Oliveira-Júnior, Jianguo Yan, Angela Melgarejo-Morales, and Punyawi Jamjareegulgarn

***Abstract*—The ionospheric storm time responses during August 2018 are investigated over South American region using multiple observables, for example, Global Navigation Satellite System (GNSS) derived vertical total electron content (VTEC) from International GNSS Service, magnetic field data, geomagnetic indices, global ionospheric maps, thermospheric mass density (TMD), and [O/N_2] ratio measurement. Strong-ionospheric and upper-atmospheric disturbances affected the ionospheric variables with long duration during the storm recovery phase and following after. First, daytime VTEC (9:00–20:00 UT) presented variations of $>$15 TECU during days 25 to 30 of August 2018 in low and middle latitudes of South America, this after sudden storm commencement (SSC). Furthermore, nighttime (21:00–24:00 and 00:00–05:00 UT) VTEC presented low values (5$<$TECU$<$7) in mid-latitude region after SSC event during the main phase, followed by high values ($>$8 TECU) in the recovery phase. Second, the ionospheric values during the storm main phase and following after, at low- and mid-latitudes, caused the equatorial ionization anomaly to expand due to prompt penetration electric field. Furthermore, VTEC enhancements are likely to occur few hours after the SSC of 25 August 2018, while enhancements of TMD and [O/N_2] ratio started to appear later on 26 and 27 of August 2018.**

***Index Terms*—Geomagnetic storm, Global Navigation Satellite System (GNSS), INTERMAGNET, ionosphere, thermosphere.**

Manuscript received April 28, 2021; revised September 22, 2021 and October 23, 2021; accepted December 7, 2021. Date of publication December 13, 2021; date of current version December 27, 2021. *(Corresponding author: Punyawi Jamjareegulgarn.)*

Munawar Shah is with the Department of Space Science NCGSA, Institute of Space Technology, Islamabad 44000, Pakistan (e-mail: shahmunawar1@gmail.com).

Ayesha Abbas is with the Department of Petroleum Engineering, NED University of Engineering and Technology, Karachi 75270, Pakistan (e-mail: ayeshaabbas01@gmail.com).

Muhsan Ehsan is with the Department of Earth and Environmental Sciences, Bahria University, Islamabad 44000, Pakistan (e-mail: muhsanehsan98@hotmail.com).

Andres Calabia Aiber is with the School of Remote Sensing and Geomatics Engineering, Nanjing University Information Science Technology, Nanjing 211544, China, and also with the Department of Physics and Mathematics, University of Alcalá Alcalá de Henares, 28801 Madrid, Spain (e-mail: andres@calabia.com).

Binod Adhikari is with the Department of Physics, St. Xavier's College, Maitighar 44600, Nepal (e-mail: binod.adhi@gmail.com).

M. Arslan Tariq and Junaid Ahmed are with the Centre for Earthquake Studies, National Centre for Physics, Islamabad 44000, Pakistan (e-mail: arslan@ncp.edu.pk; junaid.ahmed@ncp.edu.pk).

José Francisco de Oliveira-Júnior is with the Institute of Atmospheric Sciences, Federal University of Alagoas, Maceió, 57051-090, Brazil (e-mail: jose.junior@icat.ufal.br).

Jianguo Yan is with the State Key Laboratory of Information Engineering in Surveying Mapping and Remote Sensing, Wuhan University, Wuhan 430072, China (e-mail: jgyan@whu.edu.cn).

Angela Melgarejo-Morales is with the Faculty of the Earth and Space Sciences, Autonomous University of Sinaloa, Culiacan 80040, Mexico (e-mail: a_mzt@hotmail.com).

Punyawi Jamjareegulgarn is with the King Mongkut's Institute of Technology Ladkrabang, Prince of Chumphon Campus, Chumphon 86160, Thailand (e-mail: kjpunyaw@gmail.com).

Digital Object Identifier 10.1109/JSTARS.2021.3134495

I. Introduction

IONOSPHERIC and thermospheric variations associated with moderate to large geomagnetic storms have been widely reported. Because of the vital role of the ionosphere for radio communication, satellite navigation, and other communication systems, the studies on upper-atmospheric perturbations due to geomagnetic storms have become very important. Moreover, during the recent century, the use of space missions to investigate upper atmosphere perturbations has attracted many researchers [1]. Ionospheric perturbations following the geomagnetic storms are caused by solar wind shock-waves that interact with the Earth's magnetic field and could last from several hours to several days after the onset of the main phase [2]. Loewe and Prölss [3] classified the depression in a geomagnetic storm through well-defined phases: initial, main, and recovery. However, these different phases can be identified by following the propagation of a Coronal Mass Ejection (CME) to the Earth's upper atmosphere [4]. Moreover, Astafyeva *et al.* [5] attributed the nightside enhancement in summer hemisphere as a combination of prompt penetration electric field (PPEF) and thermospheric storm circulation, triggered by disturbance dynamo electric field (DDEF). On the other hand, in the summer hemisphere, daytime variations are the consequence of abnormal ionospheric variations driven by PPEF during storm main phase, while in winter hemisphere, these are caused by storm-time enhanced thermospheric composition.

The solar storm morphology and its mechanism of propagation in space have been improved by the efforts of space pioneers during the last decades. Geomagnetic storms are likely to be induced by three different solar winds: corotating intense streams, interflow from coronal holes, and rapid flows from CME [6]. The responses of the Earth's magnetosphere to solar wind variations drastically change under different interplanetary magnetic field

(IMF) conditions and can produce geomagnetic storms. This results in the penetration of electric fields that can enhance and deplete vertical total electron content (VTEC) [7]. In addition, the continuous and rapid flow of solar winds compresses the Earth's magnetosphere and high energy particles precipitate to the thermosphere normally at high latitudes. As a result, chemical, thermal, and electrodynamic variations occur in the thermosphere, ionosphere, plasmasphere, and magnetosphere [8]. For instance, by observing storm-time variations in the thermosphere, the enhancement and depletion of neutral density ratio [O/N_2] may lead to the increase and/or decrease of ion loss rate during storm-time changes [5], [9]–[10]. Moreover, there are also different studies on storm time variations in the ionosphere [26]–[27].

Several studies have reported that geomagnetic storms induce ionospheric disturbances presented by statistical analyses and different case studies [8]–[9], [11]–[13]. For example, Mansilla and Zossi [12] reported VTEC enhancement at equatorial and low latitude regions due to PPEF during the main phase of the storm on north side of the magnetic equator. Moreover, some studies mainly focused on storm-time ionospheric variations on global level and specifically emphasized on different morphological characteristics of the storm in ionosphere. Upper atmosphere variables, e.g., electron density, magnetic field, stratified electron temperature, height of F2 layer, among other, are used to monitor the responses of the upper atmosphere to geomagnetic storms [8]. Likewise, there have been many discussions about morphologies and mechanisms concerning upper atmosphere variations induced by solar storms [13]. Fortunately, upper atmosphere satellite measurements allow us to monitor and model the ionosphere at a global scale and with high temporal and spatial resolutions, thus providing high-quality observables and models [14]–[15]. Several studies use Global Navigation Satellite System (GNSS)–VTEC to highlight global and local features of ionospheric anomalies, providing new hypotheses and insights for storm-time forecasting [16].

These TEC studies have been considered essential for studying the positive and negative phases of ionospheric storms. Similarly, integrated approaches of thermosphere and magnetospheric variations related to ionospheric storms have been reported in [5]. TEC variations significantly affect the performance of satellite communication and GNSS. Despite the numerous studies on upper atmosphere processes under storm-time conditions, the modeling and forecasting of precise TEC continues to be a challenge for practical applications [17], [18]. In this sense, upper-atmospheric variations can be modeled with GNSS TEC observables in conjunction with other satellite measurements (e.g., mass density from drag on satellites [19], on-board magnetometers, etc.) over local and global scales. The main objective is to provide more evidences for better understanding the complex processes in the ionosphere–thermosphere system during storm-time conditions.

In this article, we investigate the ionospheric–thermospheric responses to the intense geomagnetic storm during August 2018 based on VTEC, magnetic field, thermospheric [O/N_2] ratio, and thermospheric mass density (TMD) over South America. This article is organized as follow: Section II describes the data and methods used in this article. Results and discussion are shown in Sections III and IV, respectively. Finally, the conclusions are given in Section V.

TABLE I
LIST OF GNSS AND INTERMAGNET STATIONS INCLUDING THEIR COORDINATES

GNSS stations					
Station Code	Geographic Coordinate		Geomagnetic Coordinate		Dip Angle
	Latitude	Longitude	Latitude	Longitude	
KOUR	06ºN	52ºW	14.91°N	21.27°E	13ºN
GLPS	05ºS	90ºW	4.18°N	17.34°W	08ºN
RIOP	08ºS	78ºW	1.59°N	5.31°W	06ºS
AREQ	15ºS	70ºW	5.34°S	2.56°E	8.1 ºS
IQQE	18ºS	69ºW	8.39°S	3.51°E	13.1 ºS
CHAPI	22ºS	45ºW	13.38°S	26.28°E	36 ºS
SANT	33ºS	71ºW	23.31°S	1.51°E	34 ºS
COYQ	45ºS	74ºW	35.29°S	1.17°W	44.8ºS
INTERMAGNET stations					
KOU	06ºN	52ºW	14.85°N	21.28°E	13ºN
HUA	12ºS	78ºW	2.44°S	5.24°W	0.8 ºS
VSS	22ºS	45ºW	13.38°S	26.28°E	38.1 ºS
PIL	33ºS	69ºW	23.32°S	3.34°E	34.7 ºS

II. DATA AND METHODS

In this article, upper-atmosphere variations due to the geomagnetic storm of August 2018 are investigated in the South American region using VTEC from 8 GNSS stations, absolute magnetic field intensity from 4 INTERMAGNET stations, space weather indices, TEC Maps from global ionospheric maps (GIMs), TMD estimated from Swarm accelerometers, and [O/N_2] ratio maps from the NASA's Global Ultraviolet Imager (GUVI). List of GNSS and INTERMAGNET stations as well as their location (e.g., geographic, geomagnetic, and dip angles) are shown in Table I, and their corresponding geographical locations are depicted in Fig. 1. In order to manifest the different morphological characteristics of the geomagnetic storm in the South American sector, the variables are studied at different scales (e.g., bihourly and daily VTEC, daily [O/N_2], etc.) and for different longitudinal sectors.

Space weather indices can provide insights about the intensity and strength of the different phases of a geomagnetic storm, including the sudden storm commencement (SSC) and the main and recovery phases. The space weather conditions are described by the IMF conditions. This paragraph refers to the geomagnetic indices used (Dst, AE, and Kp) and IMF Bz conditions. The space weather indices were obtained from the International Service of Geomagnetic Indices (ISGI) website[1] and the OMNI web Service.[2]

We used the TEC measurements to analyze both pre and poststorm conditions of the ionosphere. Slant TEC (STEC) was obtained by the geometry-free linear combination of the code or carrier-phase measurements [15]. The STEC is estimated from the enclosed electrons in a square of (1×1) m^2 tube along the light of sight between the transmitter and receiver. It is measured

[1][Online]. Available: http://isgi.unistra.fr/data_download.php
[2][Online]. Available: https://omniweb.gsfc.nasa.gov

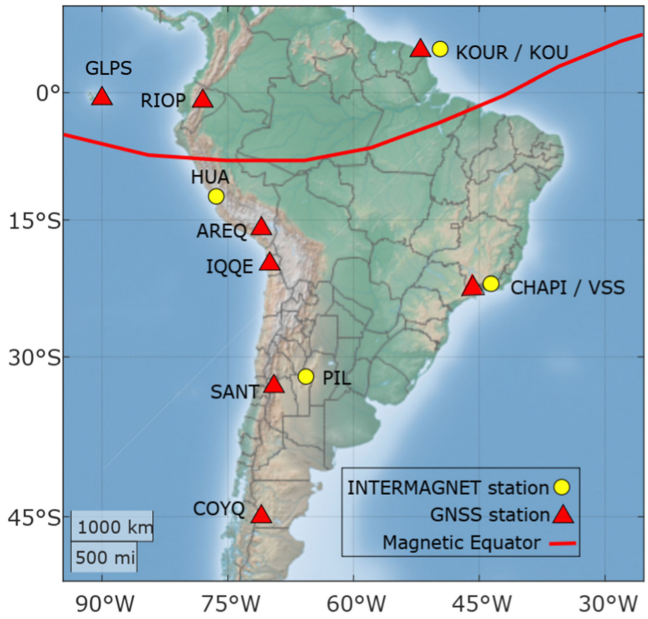

Fig. 1. Geographical locations of the GNSS and INTERMAGNET stations in the South America.

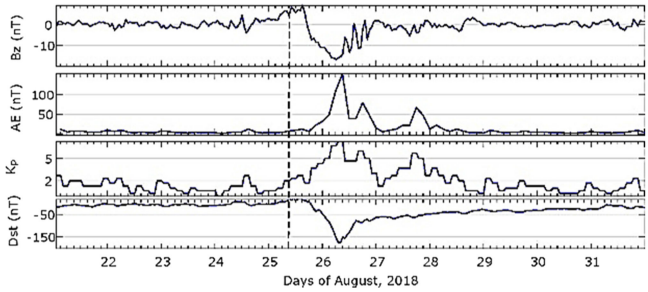

Fig. 2. Variations of gomagnetic storm indices during the storm of August 2018. The SSC is shown by a black dashed line.

in unit of TEC, where 1 TECU $= 10^{16}$ electron/m^2. The STEC is transformed to VTEC by a mapping function [20], as follows:

$$\mathrm{STEC}_a^h = \frac{-\left(f_1^2 f_2^2\right)}{40.3\ \left(f_1^2 - f_2^2\right)} \left(P_{(4,a)}^h - c.\mathrm{DCB}_a - c.\mathrm{DCB}^h\right) \tag{1}$$

$$\mathrm{VETC} = \mathrm{STEC} \times \cos\left(\arcsin\left(\frac{R\sin z}{R+H}\right)\right). \tag{2}$$

In above equations, (f_1, f_2), $P_{(4,a)}^h$, and c are GPS dual frequencies, difference of smooth code measurements, and light speed, respectively. Similarly, DCB_a and DCB^h are differential code bias for GPS satellite and ground based receiver, respectively [15]. Also, the H is for ionospheric thin shell height (in this case, $H = 350$ km), R is for radius of the Earth, and z is satellite Zenith angle. The International GNSS Service (IGS) provides GIM TEC as a derived product from the worldwide GNSS network. Each GIM map covers the Earth's longitudes ($\pm 180°$) and has a latitudinal extension of $\pm 87.5°$, with a time resolution of 2 h [15], [20]. This corresponds to a spatial resolution of $5.0° \times 2.5°$ in longitude by latitude, respectively. In this article, we compute differential TEC by subtracting one-month median TEC from an observed GIM map during August 2018 in bihourly resolution format.

The thermospheric variation before, during, and after the geomagnetic storm of August 2018 is studied from the measurement of [O/N$_2$] composition maps retrieved from OI 135.6 and LBHS radiances measured by GUVI. The GUVI is mounted on thermosphere, ionosphere, mesosphere energetics, and dynamics (TIMED) satellite since 2001 at 625 km altitude [22]. The GUVI is used to measure the thermospheric [O/N$_2$] maps during the dayside orbits that are available on.[3]

Swarm was the fifth Earth Explorer mission approved in European Space Agency's Living Planet Programme and included three identical Swarm satellites (A, B, and C), which were launched on 22 November, 2013 into a nearly polar orbit. Among other instruments, each Swarm payload included an accelerometer to measure nonconservative forces, which in turn can be used to derive TMD. Swarm mass density data can be accessed via Delft University of Technology at.[4]

III. Results

The severe geomagnetic storm of 26 August 2018 occurred as a result of an Earth directed CME [23]. The storm started mainly on 26 August 2018 and it ended on 28 August 2018. The onset of the storm SSC was at 09:00 UT and the main phase started at ~18:00 UT on 25 August 2018, and the Dst index reached −174 nT during the main phase, when the IMF-Bz was minimum at approximately 06:00 UT on 26 August 2018. Fig. 2 shows the variations of the geomagnetic indices Dst, Kp, and AE, and the IMF-Bz component, with the start of the SSC identified by a dashed vertical line.

Fig. 3 shows the hourly variations of absolute magnetic field activity during the geomagnetic storm on 25–28 August 2018. The KOU, HUA, VSS, and PIL INTERMAGNET stations are used to investigate the strength and phases of the geomagnetic storm. The magnetic field range clearly increases in all the stations after the SSC. Since the VSS and PIL stations are located at a similar magnetic latitude, the same fluctuations can be seen during all phases of the storm event. The other stations show a latitudinal dependence during the disturbed conditions. For instance, the HUA station (located at the magnetic equator) shows values near to 50 nT during initial phase and a peak of >100 nT during main and recovery phases, which demonstrates an enhanced equatorial ionization anomaly (EIA) along the magnetic equator. Moreover, the low latitude magnetic stations show abnormal values immediately after the SSC (30–40 nT).

In Fig. 4, the VTEC obtained from several IGS GNSS stations in South America also presented strong variations during the storm. VTEC for the whole month of August, 2018 is showed

[3][Online]. Available: http://guvitimed.jhuapl.edu/data_products
[4][Online]. Available: http://thermosphere.tudelft.nl

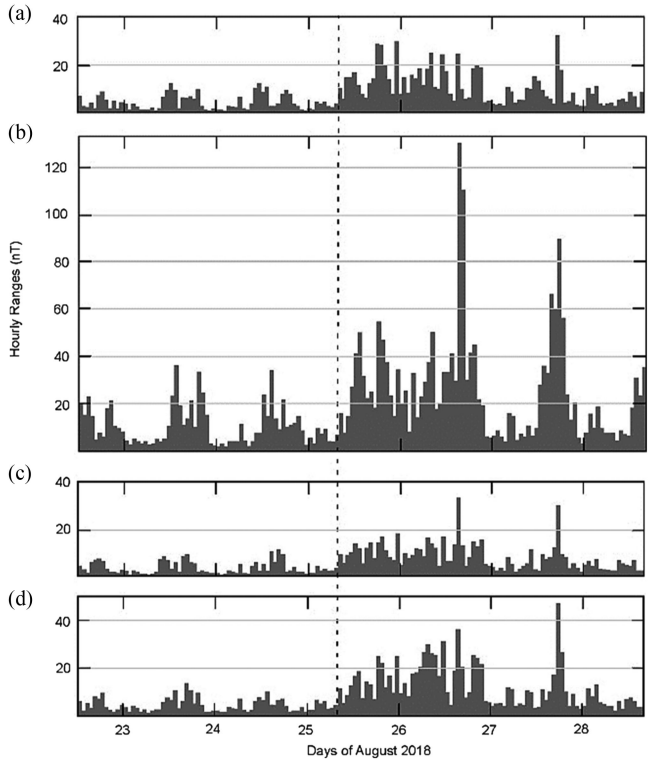

Fig. 3. Hourly variations of absolute magnetic field activity (unit: nT) obtained from magnetometers at INTERMAGNET stations during geomagnetic storm days in August 2018. The SSC is showed by black dashed line.

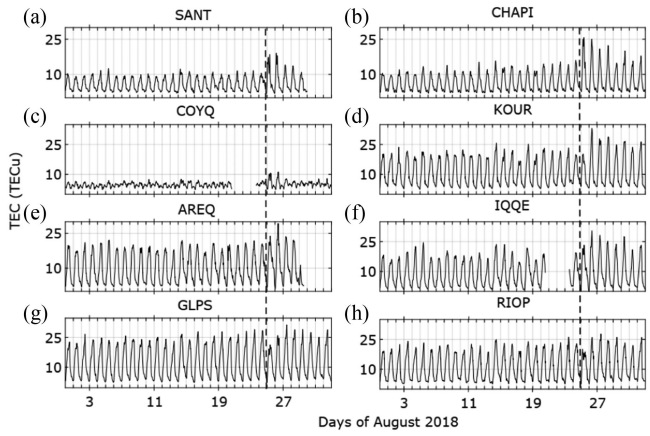

Fig. 4. Ionospheric VTEC from eight GNSS stations in South America during August 2018. The SSC is shown with a black dashed line.

to clearly illustrate the variations during storm days and non-storm days. The VTEC shows depletion immediately after the SSC commencement at equatorial regions [Fig. 4(d), (g), and (h)], followed by sudden enhancement during the main phase. Similarly, intermediate enhancements in VTEC are recorded at low-latitude GNSS stations after SSC [Fig. 4(e)–(f)] and sharp perturbed VTEC values happen at low-latitude GNSS stations after SSC [Fig. 4(a)–(c)]. On the other hand, sharp VTEC enhancement occurs during main phase of the storm in all stations (e.g., equator-low and mid-latitude). Moreover,

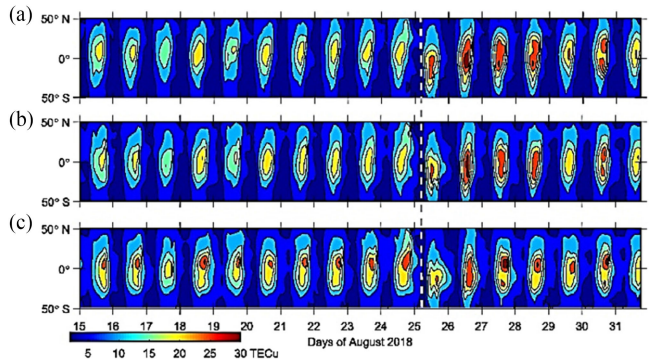

Fig. 5. Latitude time TEC from GIM profiles at (a) 40°W, (b) 60°W, and (c) 80°W during August 2018. Black dashed line is for SSC.

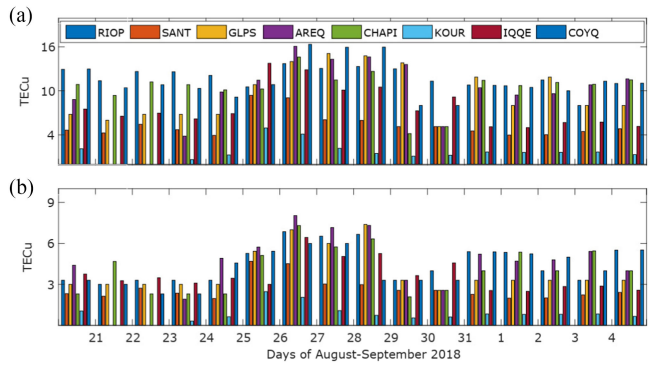

Fig. 6. Day and nighttime VTEC from eight GNSS stations in South America from 21 August 2018 to 04 September 2018.

the longitudinal profiles of VTEC (40°W, 60°W, and 80°W) show irregular geomagnetic storm variation in South America as illustrated in Fig. 5. The latitudinal profiles show a low response of VTEC before the SSC in 40°W and 60°W sectors, followed by a sharp VTEC enhancement on 26 August during the storm main phase. The main and recovery phases of the geomagnetic storm induced high VTEC values and it lasted until 31 August. High VTEC values are seen in the southern hemisphere. On the contrary, low perturbations are seen at 80°W on 26 August [Fig. 5(c)] where a latitudinal VTEC shift occurs before and after the SSC. At 80°W, the enhanced VTEC is seen at northern hemisphere before the initial phase. Then, a drastic latitudinal shift of VTEC distribution occurs from the northern to southern hemisphere.

Fig. 6 shows the diurnal analysis of ionospheric VTEC from the GNSS stations in South America. In this figure, the daytime variation of VTEC reaches up to 4–5 TECU with respect to the normal diurnal pattern (enhanced EIA dominated by PPEF at low latitude and DDEF at middle latitude), while the nighttime values are only 2–3 TECU (due to sporadic E layer). As sporadic E layer is the only layer visible at night and spread abnormally during geomagnetic days. Also, it was noted that low latitude stations have abnormal depletion, and middle to high latitude stations exist enhancement immediately after SSC. Moreover, VTEC enhancements are seen in the main and recovery phases of all the stations during 26–27 August 2018.

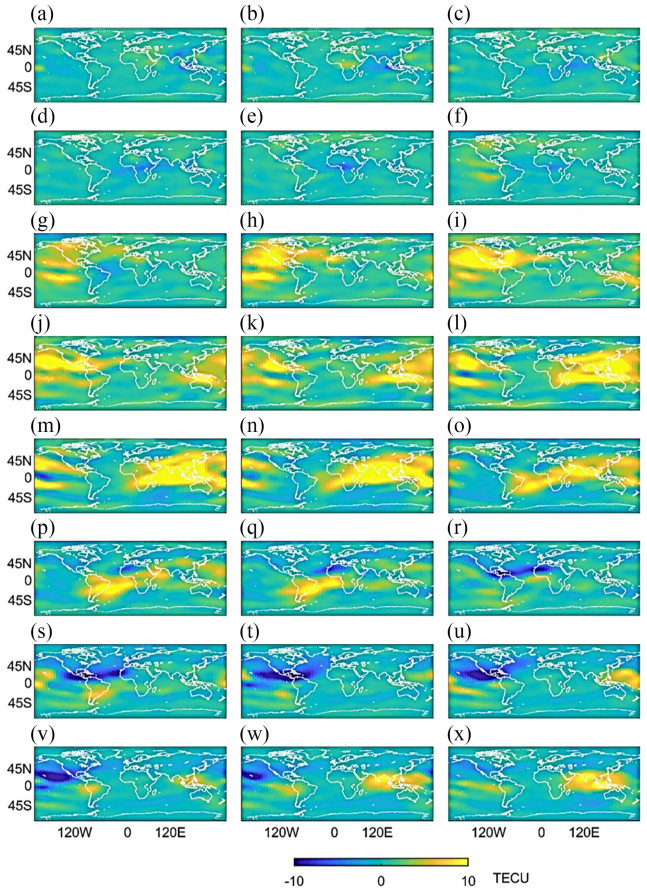

Fig. 7. Residual of GIM VTEC versus geographic coordinates during 25–27 August 2018. It is obtained by subtracting one-month GIM from a study bihourly map.

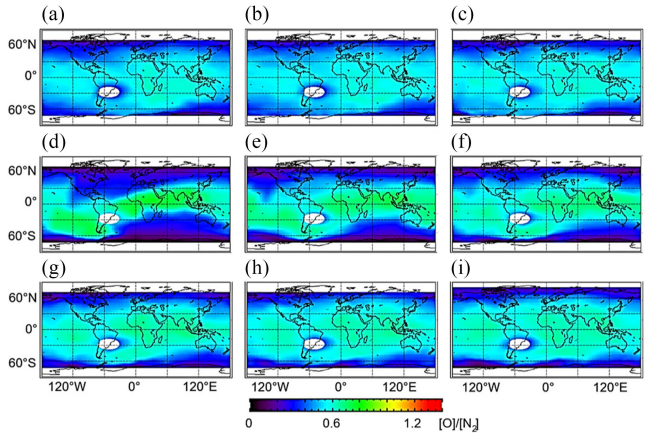

Fig. 8. Global thermospheric $[O/N_2]$ ratio maps from TIMED GUVI during the geomagnetic storm of August 2018.

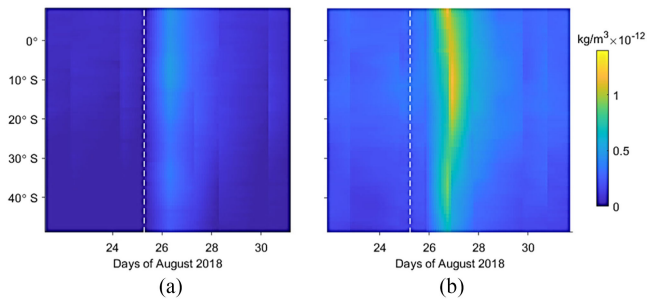

Fig. 9. Latitude profiles of thermospheric mass density (TMD) during geomagnetic storm of August 2018 over South America. The SSC is indicated with a dashed line.

Fig. 7 shows the GIM TEC during 25–27 August 2018 in bihourly format, which is obtained by subtracting one-month median of GIM from an observed map of a specific bihour. VTEC enhancements and depletions are also represented in yellow and blue regions, respectively. Fig. 7(a)–(e) shows the quiet VTEC until 25 August at 16:00 UT. The enhanced VTEC is visible from the initial phase of the storm until 26 August at 12:00 UT. After few hours on the same day, the recovery phase of the storm begins. From this point, the VTEC depletions are clearly seen more prominent in central South America until 27 August at 06:00 UT.

The daily $[O/N_2]$ ratio from GUVI–TIMED during 23–31 August 2018 shows prominent storm day variation as depicted in Fig. 8. In Fig. 8, high latitude regions show $[O/N_2]$ depletion during main phase of the storm (i.e., 26 August). On the other hand, in the low- and mid-latitude regions, the $[O/N_2]$ ratio enhances during the same period. During the quiet period before the storm, the values of $\sim$0.6 and $\sim$0.4 can be seen at the low and high latitudes, respectively. These values remain stable until 26 August at 12:00 UT. Then, in response to the storm, the $[O/N_2]$ ratio increases up to $\sim$0.9 at the low- and mid-latitude and decreases down to $\sim$0.2 at the high latitude. These values remain until 28 August at 12:00 UT, when the $[O/N_2]$ ratio retains its normal conditions. During the storm conditions, the distribution of the $[O/N_2]$ ratio is clearly aligned along the geomagnetic equator.

Fig. 9 shows the latitudinal responses of TMD to the geomagnetic storm conditions of August 2018 over South America. Note that the number of TMD used in this article is estimated from Swarm-C accelerometers ($\sim$450 km altitude). This figure shows the South American longitudes ($\sim$60°W) at the night and day sectors, approximately at 03:00 and 15:00 local solar time, respectively. Density enhancements are clear after the SSC, and are more prominent during the daytime than nighttime. During the quiet period prior to the storm, both $\sim 0.1\times10^{-12}$ and $\sim 0.5\times10^{-12}$ kg/m^3 can be seen during the night and day sectors, respectively. Then, during the main phase of the storm, these values increase up to $\sim 0.5\times10^{-12}$ and $\sim 1.5\times10^{-12}$ kg/m^3, respectively.

In addition to other analyses, the cross-correlation is also implemented on VTEC–VTEC and VTEC–solar storm indices to find variations during ionospheric storm days. The cross-correlation clarifies the storm time ionospheric of one station in all other stations. A good correlation has a value of more than $+0.5$ or -0.5, while a strong correlation has values in the range of $(+\ 0.7\pm1)$. Fig. 10 depicts the cross-correlation coefficients of VTEC computed between AREQ station with other stations during 26–27 August, 2018. The cross-correlation is applied only on the VTEC data of 26–27 August, 2018 during storm

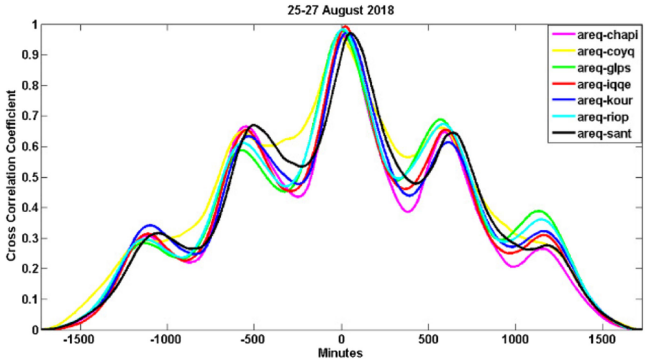

Fig. 10. Cross-correlation coefficients of VTEC calculated between AREQ station and other seven stations during intense storm on 25–27 August 2018.

main and recovery phase days where -50 nT $<$ Dst $<$ -150 nT. The x-axis represents a time duration ranging from -1500 to $+1500$ min from storm highest value (Dst $<$ -150 nT) and the y-axis represents the cross-correlation coefficients ranging from 0 to 1. The cross-correlation coefficients of VTEC between AREQ station and other seven stations: CHAPI, COYQ, GLPS, IQQE, KOUR, RIOP, and SANT are showed with different colored solid lines. Most of the stations show identical features with perfectly overlapping being the highest positive correlations of approximately 0.98 at zero-time lag. The results illustrate that the AREQ station was in same phase with other stations during the intense storm time, and each station showed identical shape between -500 and $+500$ min with a noticeable peak ($\pm$ 500 min are approx. 8 h from the peak Dst $<$ -150nT h). Note that the AREQ–IQQE curve (red line) showed a perfect overlapping nature, representing the highest correlation coefficient of approximately 0.999 at zero-time lag.

Likewise, the cross-correlation coefficients between VTEC and different geomagnetic indices: 1) IMF-Bz, 2) Dst index, and 3) Kp index for all eight GNSS stations during intense storm on 25–27 August 2018 were also computed and are shown in Fig. 11. Note that this analysis is implemented on the data of one day before and after the hour of Dst $<$ -150 nT. Here, a star and several solid lines (pink, yellow, green, red, blue, sky blue, and black) were used to represent the cross-correlation coefficients between VTEC and individual geomagnetic indices for all eight GNSS stations. In Fig. 11(a), it can be seen that the cross-correlation coefficients of IMF-Bz over AREQ station (star) and the other stations demonstrated abnormal variations during the storm days. The IMF-Bz over GLPS and RIOP stations shows perfectly negative correlation approximately 0.6 at $+20$ h. Although at zero-time of time lag, the value was approximately -0.45. The IMF-Bz over other stations correlated fairly with their VTEC values. Besides GLPS and RIOP stations, other stations show more negative fluctuations without significant correlation coefficients. These results imply that the IMF-Bz was inversely proportional to the VTEC and it seems to be the primary cause for the onset of geomagnetic storm. Moreover, in Fig. 11(b), the cross-correlation coefficients of Dst-COYP (yellow line), Dst-KOUR (blue line), and Dst-CHAPI (pink line) were negative correlations of approximately 0.8, 0.7, and 0.65 at

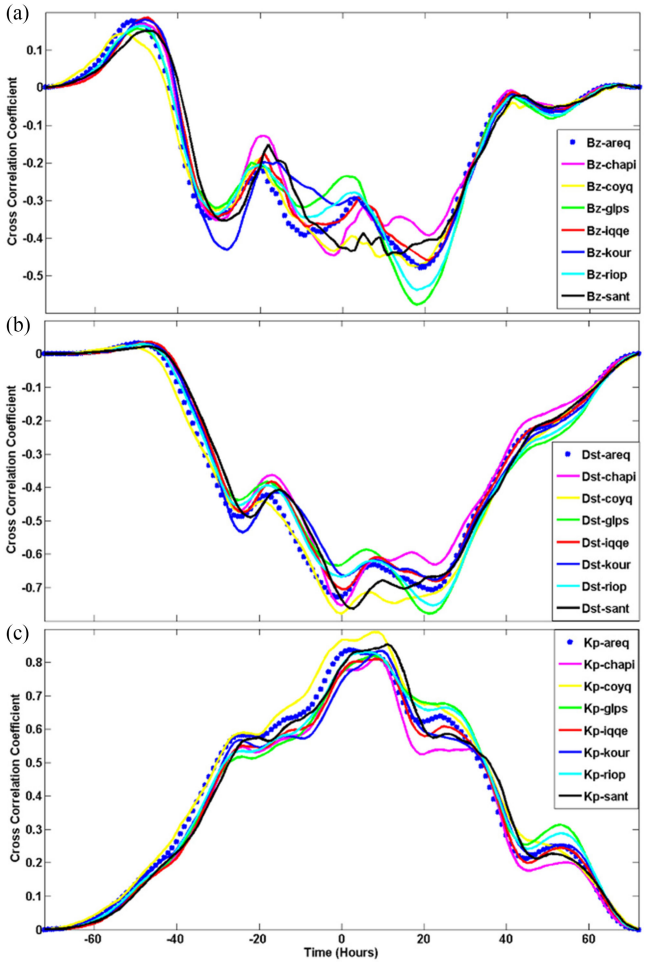

Fig. 11. Cross-correlation coefficients between VTEC values and different geomagnetic indices: (a) IMF-Bz, (b) Dst index, and (c) Kp index, for all eight GNSS stations during intense storm on 25–27 August 2018.

zero-time lag, respectively. Meanwhile, Dst-GLPS (green line) and Dst-RIOP (sky blue line) were also negative correlations of approximately 0.75 and 0.7 at time lag of $+20$ h, respectively. However, the Dst-SANT (black line) showed a negative correlation of approximately 0.75 at time lag of 1 h. Refer to Fig. 11(c), we can see the exact overlapping of Kp index with the VTEC at zero-time lag during the extreme storm, and the maximum positive value of cross-correlation coefficient was of approximately 0.85. Therefore, it can be suggested that the Kp index presented the same phase as the VTEC. This also supports the strong correlation between Kp index and VTEC.

IV. Discussions

The geomagnetic storm of August 2018 generated the intensified values detected in different variables of the upper atmosphere over South America. These variations were observed in the analysis of different ground and satellite observations during 25–26 August 2018 in this article. After the SSC, the INTERMAGNET stations over middle latitude (VSS and PIL) presented minor magnetic field enhancements than

the ones located over low latitude (KOU and HUA). All INTERMAGNET stations exhibited low values during main phase on 26 August followed by high values during the recovery phase [Fig. 3(c)–(d)]. High magnetic field values are developed immediately over low latitude stations after the SSC during main and recovery phases in South American sector. Mansilla and Zossi [12] reported small negative ionospheric responses at equator sector during main phase, which is in good agreement with the results in this article and concluded that VTEC depletion was caused by PPEF. Moreover, Macho *et al.* [24] reported daytime VTEC enhancements at low latitudes in the beginning of main phase storm, which occurred during local afternoon, and this enhancement were attributed to the effect of PPEF.

The initial phase started the South American region on 25 August during daytime, followed by the main phase in nighttime on 26 August, and then the recovery phase commenced during afternoon on 26 August. After SSC on August 25 at 17:06 UT, the mid-latitude GNSS stations reported enhancement in ionospheric VTEC values, and lasted until the recovery phase as illustrated in Fig. 4(a)–(c). Meanwhile, VTEC depletion at low-latitude GNSS stations was reported immediately after the SSC. Afterwards, the VTEC enhancement is observed during main and recovery phases of the storm in low- and mid-latitude stations on 26 August 2018, as depicted in Fig. 4. In this article, the VTEC from the stations near the equator shows depletion during the storm days in South American sector, as showed by Mansilla and Zossi [12] for equator stations in South America. They showed the phenomena due to PPEF. Macho *et al.* [24] demonstrated the uplifted EIA crest to mid-latitude regions by dominant daytime PPEF process, triggering increase VTEC during main phase of the storm followed by recovery phase.

The VTEC at three different longitudinal sectors over the South American sector shows $<$20 TECU at 40°W and 60°W before the SSC, and $>$25 TECU on August 26 during main and recovery phases [Fig. 5(a) and (b)]. The high VTEC values ($>$25 TECU) prevail to 30 August at 40°W and 60°W sectors. These high values of VTEC happened after SSC during the first few hours of main phase on the daytime sector in the southern hemisphere due to PPEF process. On the contrary, 80°W longitude possesses high VTEC values before and after the storm during 16–31 August 2018 [Fig. 5(c)]. This is due to both equatorial electrojet (EEJ) and counter electrojet (CEJ) for different local time of ionospheric storm and South Atlantic Magnetic anomaly in east sector of South America [28]. Astafyeva *et al.* [4] correlated ionospheric storm variations in Peru with EEJ depletions in western part of South America. On the other hand, Spogli *et al.* [28] reported east sector variations by EEJ followed by CEJ on 26 August. Only a slight VTEC abnormal value stimulated to southern hemisphere on August 26–27, 2018 during main and recovery phases. Then, VTEC values of $>$15 TECU moved back to northern hemisphere beyond August 27 to August 30, 2018. Additionally, storm-time variations occurred in ionospheric plasma convection, magnetic field, and thermospheric winds strength and orientation due to asymmetries in north and south hemispheres [25].

The daytime VTEC have shown post-storm variations larger than 15 TECU at the ground-based stations over low and middle latitudes in South America, which is due to enriched EIA [Fig. 6(a)]. The nighttime low latitude has shown lower VTEC variations ($5<$TECU<7) between the SSC and the main phase, and high VTEC variations ($>$8 TECU) during the recovery phase in all stations. The overall depletions in the nighttime VTEC [y-axis range of Fig. 6(b); $6<$VTEC<9] as compared to daytime [y-axis range of Fig. 6(a); $9<$VTEC<16] at low and middle latitude stations in South America occur due to lower ionization but active ionosphere with the sporadic E layer as shown in Fig. 6(b). In addition, VTEC enhancements can be seen in the low and middle latitudes of South America during 12–16 UT on August 26 during the storm main phase (Fig. 7: panels. O-Q). VTEC value exceeds more than five TECU during the main phase and immediately shifts to low VTEC values after the recovery phase of the storm. The dayside VTEC values intensify stronger than the nighttime. The nighttime VTEC enhancements were only limited to 28 August, and the daytime enhancements lasted until 30 August 2018. This shows that high latitude heating drives meridional winds toward the equator, and these move TMD enhancements to lower latitudes.

Figs. 8 and 9 have shown the thermospheric [O/N_2] ratio and the neutral mass density variations before and after the SSC. These variables enhanced during the main and recovery phases of the storm, while VTEC enhancements started earlier on 25 August as illustrated in Figs. 4–7. In fact, the model simulations of Crowley *et al.* [10] showed that the [O/N_2] ratio disturbances during storm periods are primarily associated with the changes of thermospheric neutral composition, and that plasma density enhancements may have a lower contribution to [O/N_2] ratio disturbances. In addition, Crowley *et al.* [10] also showed that the positive ionospheric storm during the 20 November 2003 storm was not related to the thermospheric neutral composition disturbances.

This article investigates upper atmosphere variations from different variables over the low and middle latitudes of South America. VTEC shows no significant ionization at high latitudes. Astafyeva *et al.* [5] pointed out that in case of poor ionization at high latitudes, meridional winds hardly transport TEC to low and middle latitudes. We have observed higher ionization over middle and low latitudes of South America than high latitudes. We also observed a hemispherical asymmetry of VTEC at 80° W, developed before and after the SSC [Fig. 5(c)]. This asymmetry is dependent on the local time variation and the direction of IMF [25].

Before the SSC, the IMF shows positive values (eastward) and then turns to negative after the SSC during the main phase as shown in Fig. 2(a). The polarity of IMF-Bz changes several on 26 August during the recovery phase of the storm. Then, the values have shown to reach 18nT at 09:00 UT on 26 August. Our analysis show that a hemispherical asymmetry occurs due to IMF Bz polarity before and after the SSC as depicted in Fig. 5(c). Low latitude variables retain a gradual increase subsequent to weak incursion of currents and the mid-latitude regions have a low ionosphere variation due to slow rate of change of magnetic field before and after the SSC.

V. Conclusion

The morphology of ionospheric and thermospheric responses to the August 2018 geomagnetic storm in South America is investigated using different datasets. We have studied the responses of the different storm phases to several observables such as VTEC, magnetic field, thermospheric [O/N_2] ratio, and TMD**.** The main findings are listed as follows:

1) The VTEC depletion is prominent at equatorial stations on north side of the magnetic equator. The reinforcement is dominant during daytime due to PPEF process in main phase of the storm over South American sector. VTEC enhancements existed at mid-latitude GNSS stations during the main phase of the storm exist immediately after the SSC due to dominant action of PPEF. Mansilla and Zossi [12] also presented one reason of increases in electron density at equatorial region during recovery phase of this storm due to neutral composition changes, which correlated with our results in this article.
2) Significant daytime VTEC during main phase of the storm on August 26, 2018 at mid-latitude GNSS stations in South American sector pointed out the dominant effect of DDEF. Moreover, the increase nighttime VTEC values ($5<$TECU<7) at low- and mid-latitude stations during main phase show the development of sporadic E due to probable particle precipitation.
3) GIM VTEC shows clearly the evidence of EIA enhancement at low and middle latitudes of South America after the SSC, especially during the main and recovery phases of the geomagnetic storm. The VTEC from GIM endorsed significant particle precipitation at low- and mid-latitudes of South America during 12:00–16:00 UT on 26 August (storm main phase). The VTEC values exceed five TECU during the main phase and immediately shift to VTEC depletion over South America during the recovery phase of the storm. Similarly, the dayside VTEC intensified stronger than the nighttime VTEC.
4) The asymmetries during the storm are seen between 40°W, 60°W, and 80°W. The VTEC enhancements persist until 30 August 2018, suggesting storm dominant feature in northern and southern hemispheres of magnetic equator in 40°W and 60°W. On the other hand, the shifting of ionospheric clouds takes place before and after SSC at 80°W.
5) The GUVI [O/N_2] maps and TMD from Swarm have shown strong daytime variations after the SSC, specifically during the recovery phase over South America. These variations followed the disturbances in the magnetic field measurements and the space weather indices. A difference of $>0.5\times10^{-12}$ kg/m^3 was found between day and nighttime TMD, estimated after the main phase of the storm.
6) The cross-correlation coefficients between VTECs and different geomagnetic indices (IMF-Bz, Dst, and Kp) implied that the solar wind dynamic pressure was the main cause of VTEC variation. The perfectly overlapping of GNSS stations on correlation analysis at zero-time lag implied that almost all the GNSS stations presented similar trends during the storm's main and recovery phases. In other words, all the GNSS stations were equally disturbed. The VTEC modification at the GNSS stations can be a consequence of ionospheric dynamics such as PPEF of the magnetospheric electric field during the main phase of geomagnetic storm. Such a VTEC variation can be the cause of magnetospheric compression and coupling mechanism; as a result, the increase in solar wind dynamic pressure causes the trapped electrons in the radiation belt.

Acknowledgment

The authors are thankful to the ISGI, NASA OMNI Web, and INTERMAGNET consortium[5] for providing different datasets. We are also thankful to IGS for GNSS VTEC and GIM data. The GUVI [O/N2] ratio data can be accessed via.[6] Swarm mass density data are accessed via Delft University of Technology website at.[7] The authors are thankful to Editor and several anonymous reviewers for their constructive comments on the article improvement.

References

[1] S. Matsushita, "A study of the morphology of ionospheric storms," *J. Geophys. Res.*, vol. 64, pp. 305–321, 1959.
[2] E. Echer, W. Gonzalez, and B. Tsurutani, "Statistical studies of geomagnetic storms with peak Dst ≤ -50 nT from 1957 to 2008," *J. Atmos. Sol. Terr. Phys.*, vol. 73, pp. 1454–1459, 2011.
[3] C. Loewe and G. Prölss, "Classification and mean behavior of magnetic storms," *J. Geophys. Res. Space Phys.*, vol. 102, pp. 14209–14213, 1997.
[4] E. Astafyeva, M. S. Bagiya, M. Förster, and N. Nishitani, "Unprecedented hemispheric asymmetries during a surprise ionospheric storm: A game of drivers," *J. Geophys. Res. Space Phys.*, vol. 125, 2019, Art. no. e2019JA027261.
[5] E. Astafyeva, I. Zakharenkova, and P. Alken, "Prompt penetration electric fields and the extreme topside ionospheric response to the June 22–23, 2015 geomagnetic storm as seen by the swarm constellation," *Earth Planets Space*, vol. 68, pp. 1–12, 2016.
[6] I. G. Richardson and H. V. Cane, "Solar wind drivers of geomagnetic storms during more than four solar cycles," *J. Space Weather Space Climate*, vol. 2, 2012, Art. no. A01.
[7] P. R. Fagundes, F. A. Cardoso, B. G. Fejer, K. Venkatesh, B. A. G. Ribeiro, and V. G. Pillat, "Positive and negative GPS-TEC ionospheric storm effects during the extreme space weather event of March 2015 over the Brazilian sector," *J. Geophys. Res. Space Phys.*, vol. 121, pp. 5613–5625, 2016.
[8] D. Buresova and J. Laštovička, "Pre-storm enhancements of foF2 above Europe," *Adv. Space Res.*, vol. 39, no. 8, pp. 1298–1303, 2007.
[9] T. Fuller-Rowell, M. Codrescu, R. Moffett, and S. Quegan, "Response of the thermosphere and ionosphere to geomagnetic storms," *J. Geophys. Res. Space Phys.*, vol. 99, pp. 3893–3914, 1994.
[10] G. Crowley *et al.*, "Global thermosphere-ionosphere response to onset of 20 November 2003 magnetic storm," *J. Geophys. Res.*, vol. 111, no. A10S18, pp. 1–9, 2006.
[11] J. Huba and S. Sazykin, "Storm time ionosphere and plasmasphere structuring: SAMI3-RCM simulation of the 31 March 2001 geomagnetic storm," *Geophys. Res. Lett.*, vol. 41, pp. 8208–8214, 2014.
[12] G. A. Mansilla and M. M. Zossi, "Ionospheric response to the magnetic storm of 22 June 2015," *Pure Appl. Geophys.*, vol. 175, pp. 1139–1153, 2018.
[13] M. Mendillo, "Storms in the ionosphere: Patterns and processes for total electron content," *Rev. Geophys.*, vol. 44, no. RG4001, pp. 1–47, 2006.
[14] M. Hernández-Pajares *et al.*, "The ionosphere: Effects, GPS modeling and the benefits for space geodetic techniques," *J. Geodyn.*, vol. 85, pp. 887–907, 2011.

[5][Online]. Available: https://www.intermagnet.org
[6][Online]. Available: http://guvitimed.jhuapl.edu/data_products
[7][Online]. Available: http://thermosphere.tudelft.nl

[15] M. Hernández-Pajares *et al.*, "The IGS VTEC maps: A reliable source of ionospheric information since 1998," *J. Geodyn.*, vol. 83, pp. 263–275, 2009.
[16] P. Galav, S. Rao, S. Sharma, G. Gordiyenko, and R. Pandey, "Ionospheric response to the geomagnetic storm of 15 May 2005 over midlatitudes in the day and night sectors simultaneously," *J. Geophys. Res. Space Phys.*, vol. 119, pp. 5020–5031, 2014.
[17] M. Klimenko, V. Klimenko, K. Ratovsky, and L. Goncharenko, "Numerical modeling of the global ionospheric effects of storm sequence on September 9–14, 2005—Comparison with IRI model," *Earth Planets Space*, vol. 64, pp. 433–440, 2012.
[18] S. Tulasi Ram *et al.*, "Duskside enhancement of equatorial zonal electric field response to convection electric fields during the St. Patrick's day storm on 17 March 2015," *J. Geophys. Res. Space Phys.*, vol. 121, pp. 538–548, 2016.
[19] S. Jin, A. Calabia, and L. Yuan, "Thermospheric variations from GNSS and accelerometer measurements on small satellites," *Proc. IEEE*, vol. 106, no. 3, pp. 484–495, Mar. 2018.
[20] J. A. Klobuchar, "Ionospheric time-delay algorithm for single-frequency GPS users," *IEEE Trans. Aerosp. Electron. Syst.*, vol. 23, no. 3, pp. 325–331, May 1987.
[21] M. A. Tariq, M. Shah, M. Hernández-Pajares, and T. Iqbal, "Pre-earthquake ionospheric anomalies before three major earthquakes by GPS-TEC and GIM-TEC data during 2015-2017," *Adv. Space Res.*, vol. 63, pp. 2088–2099, 2019.
[22] A. Christensen *et al.*, "Initial observations with the global ultraviolet imager (GUVI) in the NASA TIMED satellite mission," *J. Geophys. Res.*, vol. 108, no. A12, 2003, Art. no. 1451.
[23] P. Vanlommel, "Solar-terrestrial centre of excellence (STCE) newsletter, 20–26 August 2018," 2018.
[24] E. P. Macho, E. Correia, C. M. Paulo, L. Angulo, and J. A. G. Vieira, "Ionospheric response to the June 2015 geomagnetic storm in the South American region," *Adv. Space Res.*, vol. 65, pp. 2172–2183, 2020.
[25] K. M. Laundal *et al.*, "North–south asymmetries in earth's magnetic field," *Space Sci. Rev.*, vol. 206, pp. 225–257, 2017.
[26] E. R. de Paula *et al.*, "Multi-technique investigations of storm-time ionospheric irregularities over the São Luís equatorial station in Brazil," *Ann. Geophys.*, vol. 22, no. 10, pp. 3513–3522, 2004.
[27] R. Hajra and S. K. Chakraborty, "Equatorial ionospheric responses in relation to the occurrence of main phase of intense geomagnetic storms in the local dusk sector," *J. Atmos. Sol. Terr. Phys.*, vol. 73, no. 7, pp. 760–770, 2011.
[28] L. Spogli *et al.*, "Ionospheric response over Brazil to the August 2018 geomagnetic storm as probed by CSES-01 and Swarm satellites and by local ground-based observations," *J. Geophys. Res.: Space Phys.*, vol. 126, 2021, Art. no. e2020JA028368.

Munawar Shah received the M. degree in geophysics from Quaid e Azam University, Pakistan, in 2013 and the Ph.D. degree in Geodesy and Geodynamics from Shanghai Astronomical Observatory, CAS, China, in 2017.

He is currently working as an Assistant Professor with the Department of Space Science, IST Islamabad, Islamabad, Pakistan. He is also affiliated with the National Center for GIS and Space Applications, IST, Islamabad, Pakistan. He has authored/coauthored many reputed journals and a book chapter. His group is working on CORS network in Pakistan for space weather monitoring. His research interests include GNSS ionospheric modeling and its applications in space weather and Earth observations.

Ayesha Abbas photograph and biography not available at the time of publication.

Muhsan Ehsan photograph and biography not available at the time of publication.

Andres Calabia Aiber photograph and biography not available at the time of publication.

Binod Adhikari photograph and biography not available at the time of publication.

M. Arslan Tariq photograph and biography not available at the time of publication.

Junaid Ahmed photograph and biography not available at the time of publication.

José Francisco de Oliveira-Júnior photograph and biography not available at the time of publication.

Jianguo Yan photograph and biography not available at the time of publication.

Angela Melgarejo-Morales photograph and biography not available at the time of publication.

Punyawi Jamjareegulgarn received the Doctoral degree from the Department of Telecommunication Engineering, King Mongkut's Institute of Technology Ladkrabang, Bangkok, Thailand, in 2017.

Since 2012, he has been an Associate Professor with King Mongkut's Institute of Technology Ladkrabang, Prince of Chumphon Campus, Bangkok, Thailand. His research interests include ionospheric irregularities, TEC modeling, RTK-based positioning, plasma bubbles, and earthquake investigations based on GPS TEC and GIM TEC.